

Observation of spin-glass behavior in homogeneous (Ga,Mn)N layers grown by reactive molecular-beam epitaxy

S. Dhar,* O. Brandt, A. Trampert, K. J. Friedland, Y. J. Sun, and K. H. Ploog
Paul-Drude-Institut für Festkörperelektronik, Hausvogteiplatz 5–7, D-10117 Berlin, Germany

(Received 7 November 2002; published 24 April 2003)

We present a detailed study of the magnetic properties of (Ga,Mn)N layers grown directly on 4H-SiC substrates by reactive molecular-beam epitaxy. X-ray diffraction and transmission electron microscopy demonstrates that homogeneous (Ga,Mn)N alloys of high crystal quality can be synthesized by this growth method up to a Mn-content of 10–12%. Using a variety of magnetization experiments (temperature-dependent dc magnetization, isothermal remanent magnetization, frequency and field dependent ac susceptibility), we demonstrate that insulating (Ga,Mn)N alloys represent a Heisenberg spin-glass with a spin-freezing temperature around 4.5 K. We discuss the origins of this spin-glass characteristics in terms of the deep-acceptor nature of Mn in GaN and the resulting insulating character of this compound.

DOI: 10.1103/PhysRevB.67.165205

PACS number(s): 75.10.Nr, 75.50.Lk, 75.50.Pp, 81.15.Hi

I. INTRODUCTION

Recently, the issue of achieving room-temperature ferromagnetism in diluted magnetic semiconductors (DMS) is gaining a lot of attention because of their importance for developing future “spintronic” devices.¹ Mn-doped III-V DMS are currently in the focus of interest, with (Ga,Mn)As being the most extensively studied compound of this class. The highest Curie temperature T_C reported for this material is 110 K. Dietl *et al.*² have calculated T_C for various Mn doped (5%) III-V semiconductors using the Zener model of carrier-induced ferromagnetism. In fact, contrary to Mn-doped II-VI DMS where Mn is an isoelectronic impurity on the group II site, Mn incorporates substitutionally on the group III site in III-V DMS and thus acts in principle as an acceptor which provides the required free carriers to turn the antiferromagnetic Mn-Mn interaction into ferromagnetic. Assuming a hole concentration of $3.5 \times 10^{20} \text{ cm}^{-3}$, this model² predicts T_C to be above 300 K in $\text{Ga}_{0.95}\text{Mn}_{0.05}\text{N}$ as compared to 120 K for $\text{Ga}_{0.95}\text{Mn}_{0.05}\text{As}$.

Several groups have thus initiated the growth and investigation of this material. The results, however, show significant discrepancies, particularly regarding the magnetic properties of the layers. For example, while some researchers have reported antiferromagnetic behavior for this material,^{3,4} others observed ferromagnetism with various different values of T_C ranging from 20 to 940 K.^{4–8} All values of T_C above room temperature stem from *n*-type or even highly resistive samples.^{5–7} The origin of the ferromagnetism observed is thus far from understood. If it were an intrinsic property of insulating (Ga,Mn)N, it is clear that the model of Dietl *et al.*² would not apply to this case. A more recent calculation based on the double-exchange mechanism in fact predicted a transition between a spin-glass and a ferromagnetic state in insulating (Ga,Mn)N for sufficiently low concentrations (<20%) of Mn.⁹ However, it is important to note that there exist several Ga-Mn and Mn-N phases, which are ferromagnetic, ferrimagnetic or antiferromagnetic in nature. Furthermore, some of these phases are ferromagnetic up to very high temperatures (for example, MnGa: ferromagnetic, $T_C > 600 \text{ K}$;¹⁰ Mn_4N : ferrimagnetic, $T_C = 738 \text{ K}$ ¹¹). The forma-

tion of such phases as precipitates during growth can dominate the magnetic properties of the material.

Recently, it has been reported that the formation of secondary phases during the growth of (Ga,M)N with molecular-beam epitaxy (MBE) is inhibited in the presence of hydrogen.¹² Reactive molecular-beam epitaxy (RMBE) might thus be a suitable technique for the growth of homogeneous (Ga,Mn)N, since growth is automatically performed in the presence of H stemming from the decomposition of NH_3 . In fact, by employing RMBE we have been able to grow homogeneous (Ga,Mn)N alloys up to a Mn content of 10%, the properties of which are the subject of the present paper. However, we have also found that clustering *does* occur at Mn contents exceeding 12–13%.¹³ These latter layers are indeed observed to be ferromagnetic up to very high temperatures (>800 K). However, this ferromagnetism is *not* an intrinsic property of these (Ga,Mn)N layers but originates from the nm-scale Mn-rich clusters formed during growth, as will be shown in detail in a forthcoming publication.¹⁴

Here, we present a detailed study of the magnetic properties of homogeneous (Ga,Mn)N layers grown directly on 4H-SiC(0001) by RMBE. All layers under investigation are insulating in nature. Using a variety of experiments (temperature-dependent dc magnetization, isothermal remanent magnetization, frequency, and field dependent ac susceptibility), we demonstrate that insulating (Ga,Mn)N alloys represent a Heisenberg spin-glass with a spin-freezing temperature around 4.5 K. To the best of our knowledge, (Ga,Mn)N is the first III-V DMS which exhibits spin-glass properties. The origin of the spin-glass behavior of (Ga,Mn)N is likely to be analogous to that discussed for the archetypal spin-glasses represented by Mn-doped II-VI DMS, namely, the simultaneous occurrence of disorder, arising from the spatially random substitution of group II element by Mn ions, and frustration of the antiferromagnetic interactions between Mn^{++} ions naturally provided by the wurtzite lattice.¹⁵

II. EXPERIMENT

The samples under investigation are grown in a custom designed two-chamber MBE system equipped with conventional effusion cells for Ga and Mn and an unheated NH_3 gas

injector. A commercial filter purifies NH_3 and a mass-flow controller adjusts its flow into the growth chamber. Semi-insulating Si-face 4H-SiC(0001) is used as substrate which is *ex situ* H_2 etched and *in situ* treated with Ga to obtain an atomically smooth and clean surface prior to growth, as described in detail in Ref. 16. The (Ga,Mn)N layers are grown directly (with one exception) on these SiC substrates at a substrate temperature of 710°C (100°C lower than the temperature normally used for GaN growth) which results in homogeneous (Ga,Mn)N layers up to a Mn content of 10%. The NH_3 flux is controlled to keep the III-V ratio constant for all layers, and resulted in a chamber pressure of $4-5 \times 10^{-5}$ Torr during growth. The Mn/Ga flux ratio was changed in order to adjust the Mn content in the layers. We focus here on two ~ 350 nm thick layers, the Mn content of which is 7.6% (sample A) and 10.3% (sample B) as measured by secondary ion-mass spectrometry (SIMS) depth profiles. Conductivity measurements reveal both samples to be electrically highly resistive ($\rho \approx 1 \text{ M}\Omega \text{ cm}$) even at room temperature. Above room temperature, thermally activated conduction sets in with an activation energy of 0.15 eV.

Nucleation and growth is monitored *in situ* by reflection high-energy electron diffraction (RHEED). Structural properties of the layers are investigated by x-ray diffraction (XRD) and transmission electron microscopy (TEM). Symmetric high-resolution triple-axis x-ray ω - 2θ scans are taken with a Bede D3 diffractometer equipped with a Cu $K\alpha_1$ rotating-anode source, a Bartels-type Ge(002) monochromator and a Si(111) analyzer. TEM is performed using a JEOL3010 microscope operating at 300 kV. The bright-field micrographs are taken with a diffraction vector $\mathbf{g}=[0002]$. The magnetization measurements are done in a quantum design superconducting quantum interference device (SQUID) setup. Magnetization loops are recorded at various temperatures for magnetic fields between ± 5 kOe. Prior to measuring the temperature dependence of the magnetization, the sample is first cooled from room temperature to 2 K either under a saturation field of 10 kOe [field cooled (FC)] or at zero field [zero field cooled (ZFC)]. For ac susceptibility measurements, an ac amplitude of 3.5 Oe is used. The magnetic field is applied parallel to the surface, i.e., perpendicular to the c axis, in all measurements. All data are corrected for the diamagnetic contribution of the substrate.

III. STRUCTURAL CHARACTERIZATION

During nucleation of the layers, a spotty RHEED pattern is initially observed reflecting a purely three-dimensional growth mode. Upon the deposition of 10 ML (Ga,Mn)N, the RHEED pattern becomes entirely streaky. Figure 1 shows the RHEED pattern along the $\langle 11\bar{2}0 \rangle$ azimuth during growth. The streaky RHEED pattern reflects a two-dimensional growth mode and a smooth surface. It is noteworthy that the pattern does not exhibit the (2×2) reconstruction which we encounter when growing pure GaN.¹⁷ This finding may be indicative of the presence of a Mn floating layer on the growth front. However, the intensity of the RHEED pattern stays constant during growth, suggesting that the Mn coverage rapidly reaches a steady-state value due to a balance of

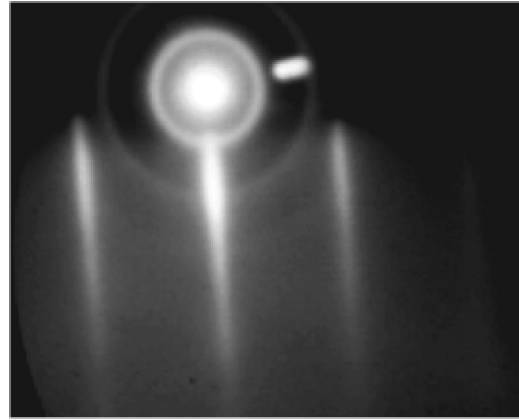


FIG. 1. RHEED pattern of (Ga,Mn)N during growth along the $\langle 11\bar{2}0 \rangle$ azimuth.

adsorption and desorption of Mn adatoms. In fact, the SIMS depth profiles show no accumulation of Mn at the as-grown surface, and the Mn content is constant over the entire depth of the layer.

The crystalline structure of these samples is studied by XRD. Symmetric (0002) and asymmetric $(11\bar{2}4)$ x-ray rocking curves for the samples under investigation exhibit a width of $300''$ and $900''$, respectively, actually lower than values we observe for equally thin pure GaN layers grown under these conditions, and comparable to values reported for high-quality GaN grown by MBE in general. The incorporation of significant amounts of Mn thus does not deteriorate the crystal quality.

Figure 2 shows a high-resolution triple-axis ω - 2θ scan of a 450 nm thick (Ga,Mn)N layer grown here on a 195 nm thick GaN buffer layer on 6H-SiC(0001). The reflections of both epilayers are clearly resolved. The simulation has been done simply by using appropriate lattice constants to match the angular position of these reflections. Note that the reflection of (Ga,Mn)N occurs at a larger angle than that of the GaN buffer layer, revealing a smaller c lattice constant for the alloy as compared to GaN. The shape of the experimental profile is described well by the simulation (for which we used an instrumental broadening of $17''$), indicating that inhomogeneous strain is virtually absent in these layers. This

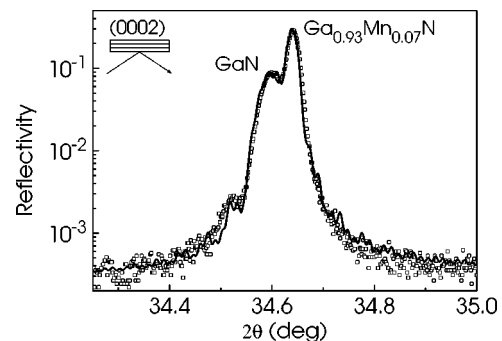


FIG. 2. Experimental (\square) and simulated (—) triple-axis ω - 2θ scan across the GaN(0002) reflection of a (Ga,Mn)N/GaN structure grown on 6H-SiC(0001). The Mn-content of the layer as indicated has been determined by SIMS.

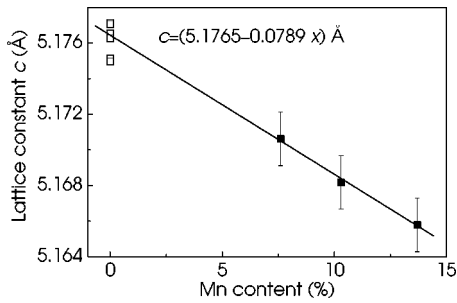


FIG. 3. Lattice constant c obtained from triple-crystal ω - 2θ scans versus Mn content. The solid squares represent (Ga,Mn)N layers. The open squares represent a number of pure GaN samples grown on 4H-SiC. The solid line is a linear fit to the data, the parameters of which are given in the figure.

finding suggests a homogeneous incorporation of Mn in the (Ga,Mn)N alloy.

In Fig. 3, we show c as a function of Mn-content for three ~ 350 nm thick (Ga,Mn)N layers grown on 4H-SiC. Solid squares represent sample A and B as well as another (Ga,Mn)N layer with 14% Mn content grown under identical conditions except for the Mn/Ga ratio. Open squares represent a number of pure GaN samples grown on 4H-SiC. The values measured for the latter samples scatter by ± 0.001 Å, which may originate in a slight variation of the substrate lattice constant due to doping inhomogeneities or a slight difference of the thermal strain in the GaN layer. In any case, despite this scatter the value of c is seen to decrease linearly with increasing Mn-content, indicating a predominantly substitutional incorporation of Mn. It is interesting to note that an opposite trend is observed for (Ga,Mn)As, where the out-of-plane lattice constant is found to increase with the Mn content.¹⁸

Figure 4 shows bright-field TEM micrographs of sample A and B. Both the samples are seen to be homogeneous layers without any evidence for a secondary phase. This finding is in contrast to layers with higher Mn content, where

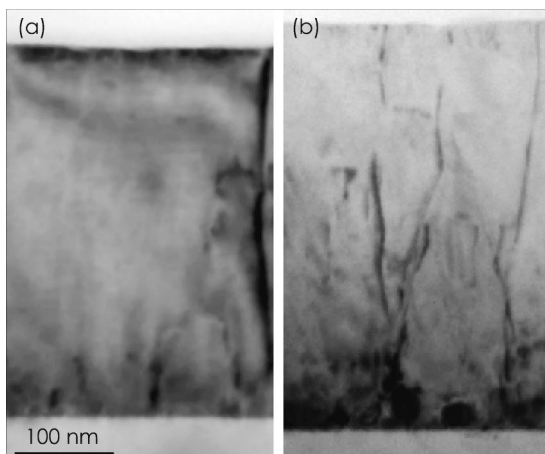


FIG. 4. Bright-field TEM micrographs of (a) sample A and (b) sample B. The contrast close to the (Ga,Mn)N/SiC interface stems from dislocation loops. The dark lines intersecting the micrographs originate from screw dislocations.

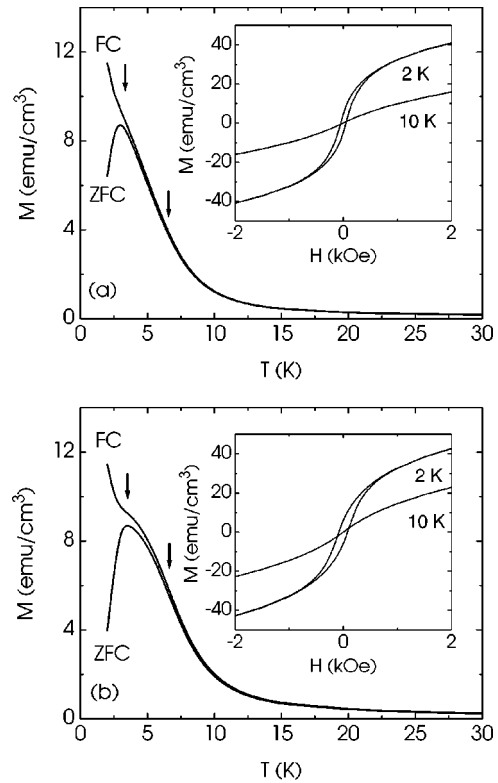


FIG. 5. Temperature dependence of field-cooled (FC) and zero-field-cooled (ZFC) dc magnetization at 100 Oe for sample A (a) and sample B (b). Arrows indicate the onset of weak and strong irreversibility. The respective insets show the magnetization loops at 2 and 10 K.

nm-size clusters are observed in the micrograph.¹⁴ We note that we were unable to detect the presence of these clusters by XRD, presumably because of their minuscule size resulting in a significant broadening of the reflection. The absence of additional reflections in XRD profiles is thus no proof for the absence of precipitates or clusters.

IV. MAGNETIZATION

A. Temperature dependence of dc magnetization

Figure 5 shows the temperature dependence of FC and ZFC magnetization curves for samples A [Fig. 5 (a)] and B [Fig. 5(b)] at a magnetic field of 100 Oe. Both samples exhibit a quite similar behavior, namely, a pronounced FC-ZFC irreversibility and a sharp cusp in the ZFC curves. These two features are fingerprints for spin-glass systems.¹⁵ A closer inspection of these curves reveals a two-step irreversible process. First, a weak irreversibility occurs at around 6 K which is then followed by a strong irreversibility close to 3 K (indicated by arrows). This two-step irreversibility has been observed in many Heisenberg spin-glasses and is commonly attributed to the freezing of transversal (weak irreversibility) and longitudinal (strong irreversibility) spins.^{19–21} The FC and ZFC curves converge above 6 K and gradually decrease with the increase of temperature, indicating paramagnetic behavior at higher temperatures. The respective insets of the

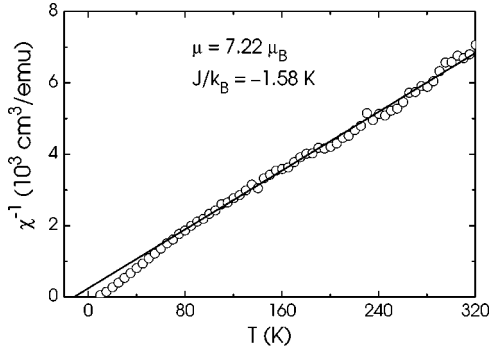


FIG. 6. Inverse dc susceptibility of sample B (at $H=200$ Oe) as a function of temperature (open circles). The straight line represents the Curie-Weiss law with $\theta=-11.4$ K.

figure show the magnetization loops at 2 and 10 K. A hysteresis is seen only below 6 K, as expected from the FC and ZFC curves.

In Fig. 6, the inverse dc susceptibility measured for sample B at $H=200$ Oe is plotted versus temperature. As expected, a clear linear dependence is found above 80 K. Above 200 K, the data scatter because the diamagnetic contribution from the substrate dominates the magnetization. We have fit the data between 80 and 200 K by the Curie-Weiss law

$$\chi = \frac{C}{(T - \theta)}, \quad (1)$$

where $C = N\mu^2/3k_B$ and $\theta = (2/3)xS(S+1)z(J/k_B)$. Here, N is the number of Mn ions per cm^3 , $\mu = g\mu_B[S(S+1)]^{1/2}$ the spin magnetic moment, x the Mn content, z the number of nearest neighbors (12 for a wurtzite lattice), and J the nearest-neighbor exchange integral. In (Ga,Mn)N, $g=2$ and $S=5/2$, as has been determined by electron spin resonance.²² The fit by Eq. (1) yields $\mu = 7.22\mu_B$ and $J/k_B = -1.58$ K. Both values are close to those obtained in Ref. 3 for a sample with similar Mn concentration. It is interesting to note that the antiferromagnetic Mn-Mn nearest-neighbor interaction in II-VI DMS is about one order of magnitude larger.²³ Furthermore, the value of μ is close to the theoretical value of $g[S(S+1)]^{1/2}\mu_B = 5.92\mu_B$. The negative value of J reflects the antiferromagnetic Mn-Mn nearest-neighbor interaction. A quantitatively similar behavior is also observed for sample A ($\theta = -10.4$ K).

B. Isothermal remanent dc magnetization

Since the properties of samples A and B are qualitatively identical, we will focus in the following on sample B. The isothermal remanent magnetization (IRM) of this sample is obtained by cooling the sample in zero field from 100 to 2 K, increasing the field to the desired value, holding it there for 5 min, then turning the field to zero and observing the remanent magnetization as a function of time. We have studied the IRM at various initial magnetic fields between 1 to 30 kOe. The remanent magnetization $M_{\text{IRM}}(t)$ decays so slowly that its value remains nonzero even after 2 h of decay. This is again a fingerprint of spin-glasses. Figure 7 shows the ex-

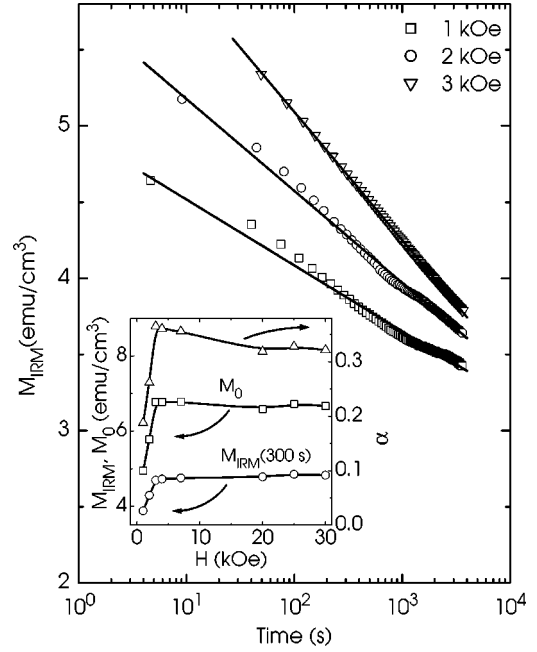


FIG. 7. Isothermal remanent magnetization in a $M_{\text{IRM}}(t)$ versus $\ln(t)$ representation. The solid lines represent the fit to the experimental data. The inset of the figure shows the dependence of the fit parameters M_0 (squares) and α (triangles) as well as M_{IRM} measured at 300 s (circles) on the magnetic field. The lines are guides to the eye.

perimental data as well as fits to them according to $M_{\text{IRM}}(t) = M_0 - \alpha \ln(t)$ at 1, 2 and 3 kOe. The fits are not perfect, but significantly better than those obtained with a stretched exponential. In the inset of Fig. 7 we show the values of the two fitting parameters M_0 and α as well as M_{IRM} at $t=300$ s as a function of the field. All these parameters increase rapidly with the magnetic field up to 3 kOe and then saturate. This behavior has been observed in several different spin-glasses²⁴⁻²⁶ and is also supported by theory.^{27,28} Furthermore, the clear correlation between M_0 and α is a manifestation of the memory of a spin-glass.

C. Frequency dependence of ac susceptibility

The temperature dependent ac susceptibility is measured at various measurement frequencies ranging from 0.1 Hz to 1 kHz. Representative examples are shown in Fig. 8. The real part χ' of the complex susceptibility exhibits a pronounced peak at a temperature T_f around 5 K. The imaginary part χ'' exhibits a sudden onset at a temperature T_i (around 6 K) slightly above T_f . This behavior is characteristic for a spin-glass: T_i indicates the onset of the weak irreversibility and is considered to be related to transversal spin freezing, whereas T_f is considered to be related to the strong irreversibility and thus to longitudinal spin freezing.²⁹ Both T_f and T_i increase with the measurement frequency (f). The frequency sensitivity of T_f is determined to be $\Delta T_f/T_f \Delta \ln f = 0.012$. This value is comparable to those reported for other canonical spin-glass systems, e.g., Cd_{0.6}Mn_{0.4}Te: 0.02 (II-VI DMS spin-glass), Cu:Mn: 0.007 (metallic spin-glass), and

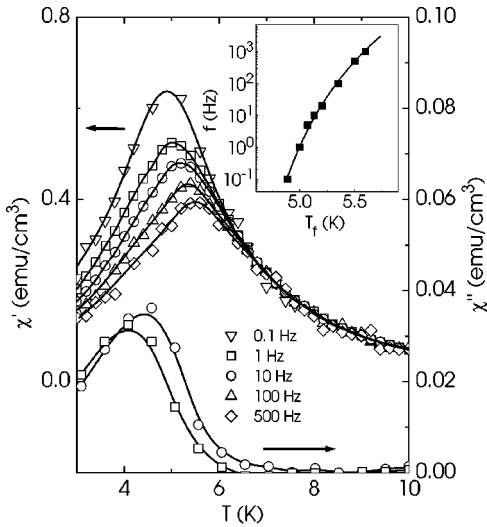


FIG. 8. Temperature variation of the real and imaginary parts of the ac susceptibility at various measurement frequencies. Curves through the data are guides to the eye. The inset of the figure shows the frequency-dependent shift of the peak position T_f of the real part. The solid curve is the fit to the data by Eq. (2).

$\text{Eu}_{0.6}\text{Sr}_{0.4}\text{S}$: 0.05 (insulator spin-glass).²⁹ Assuming a phase transition at T_0 , the spin freezing can be analyzed in terms of a critical slow down above T_0 using the following expression:^{29–31}

$$f\tau_0 = A \left[\frac{T - T_0}{T} \right]^{-z\nu}, \quad (2)$$

where ν is the critical exponent for the correlation length ξ , and z is the dynamic exponent relating f to ξ by $1/f \cong \tau_0 \xi^z$. The experimental variation of $T_f(f) \equiv T$ has been analyzed using Eq. (2) as shown in the inset of Fig. 8. We obtain a phase transition temperature $T_0 = 4.5$ K, $z\nu = 10$ and $\tau_0 \approx 10^{-11}$ s. The shortest relaxation time τ_0 compares well with $\hbar/k_B T_0 = 1.68 \times 10^{-12}$ s. The value of $z\nu = 10$ is close to the values ($z\nu \approx 8-10$) reported for the spin-glasses $\text{Cd}_{0.6}\text{Mn}_{0.4}\text{Te}$ (Refs. 29,32) and $\text{Eu}_{0.6}\text{Sr}_{0.4}\text{S}$.³³ It also agrees well with the simulation of Ogielski³⁰ for 3D spin-glasses with short-range interaction.

D. Magnetic field dependence of ac susceptibility

In a Heisenberg spin-glass, both strong and weak irreversibility lines are predicted to follow a $\tau = ch^a$ behavior, with the reduced temperature $\tau = [1 - T_{f,i}/T_0]$, the reduced magnetic field $h = \mu H/k_B T_0$ where T_0 is the transition temperature, a pre-factor c and a simple fraction or an integer a . In an ideal 3D-Heisenberg spin-glass without any anisotropy, the weak irreversibility line related to the freezing of the transversal spin components (perpendicular to the applied field) is predicted to follow a Gabay-Toulouse-(GT)-like behavior with $\tau \propto h^2$, whereas the strong irreversibility line related to the freezing of the longitudinal spin components is expected to be DeAlmeida-Thouless-(AT)-like with τ

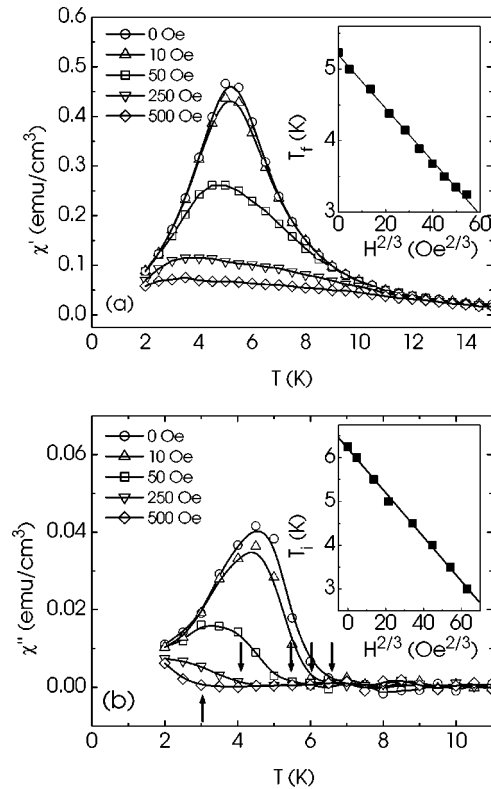


FIG. 9. Temperature variation of the (a) real and (b) imaginary part of the ac susceptibility at various dc fields. T_f and T_i (solid squares) are plotted versus $H^{2/3}$ in the insets of (a) and (b), respectively. The solid lines show linear fits to the data.

$\propto h^{2/3}$.³⁴ This behavior has been observed in various well-characterized Heisenberg spin-glass systems [such as, e.g., $\text{Cd}_{1-x}\text{Mn}_x\text{Te}$ (Ref. 29)].

Figures 9(a) and 9(b) show the temperature dependence of the real and imaginary part of the complex susceptibility measured at various dc magnetic fields from 0 to 500 Oe with 10 Hz of ac frequency. T_f and T_i (indicated by arrows) decrease with increasing dc field. $T_f(H)$ shows AT-like behavior, as expected for a Heisenberg spin-glass as seen from the inset of Fig. 9(a). However, $T_i(H)$ does not follow a GT-like behavior as expected for an isotropic Heisenberg spin-glass. $T_i(H)$ rather exhibits a strong dependence on H as is evident from a much larger variation of T_i with H compared with, e.g., $\text{Cd}_{0.45}\text{Mn}_{0.55}\text{Te}$ [where $T_i(H)$ indeed exhibits a GT-like behavior]. For $\text{Cd}_{0.45}\text{Mn}_{0.55}\text{Te}$, the observed variation of T_i is reported to be of the order of 10^{-2} K²⁹ for a change in H of 100 Oe, whereas in the present case the change is several Kelvin. In fact, $T_i(H)$ is observed to follow a $H^{2/3}$ dependence, as shown in the inset of Fig. 9(b). A similar behavior (AT-like) of the weak irreversibility line has been observed in $\text{Eu}_{0.4}\text{Sr}_{0.6}\text{S}$ which has been attributed to a large local anisotropy energy of 0.4 K present in this particular Heisenberg spin-glass.³³ If the anisotropy is large, the anisotropy parameter $d = D/J$, where D is the mean anisotropy energy, plays a crucial role in determining the behavior of the irreversibility lines. It has been shown theoretically that the weak irreversibility line can

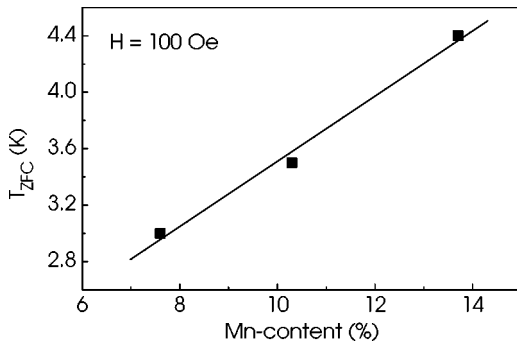


FIG. 10. Peak positions of the temperature dependent ZFC magnetization curves measured at 100 Oe as a function of Mn concentration. The solid line is a guide to the eye.

show AT-like behavior if $d \gg h^{2/3}$.³⁵ An accurate determination of d in the present sample is not possible because of our lack of knowledge regarding the various sources of anisotropy present in the crystal. However, a lower-bound estimate of d is obtained by calculating the dipolar anisotropy D/k_B [$D = \mu^2/r^3$ with $r = (3/4\pi N)^{1/3}$] which turns out to be 0.6 K, similar to the value observed for $\text{Eu}_{0.4}\text{Sr}_{0.6}\text{S}$ (0.4 K). The minimum value of d is thus 0.38, significantly larger than the value of $h^{2/3} = 0.14$ for the maximum dc field (500 Oe) used in our experiments.

A qualitatively identical behavior as reported above is seen also for samples with lower and higher Mn content (the latter of which exhibit Mn-rich clusters that additionally give rise to ferromagnetism at high temperatures). The main difference between these samples is the spin-freezing temperature, which is found to increase with the Mn-content as shown in Fig. 10 even for the sample incorporating clusters. In fact, the volume fraction of these clusters is very small ($<1\%$),¹³ and the overwhelming majority of Mn atoms continue to occupy substitutional sites in the matrix as also indicated by the monotonous change of the lattice constant (see Fig. 2). The spin-glass character of (Ga,Mn)N is thus preserved even when precipitation occurs.

The dramatic difference in the magnetic properties of the insulating spin-glass (Ga,Mn)N and the metallic ferromagnet (Ga,Mn)As appears puzzling at the first glance, but is easily explained. In the absence of free carriers, the Mn-Mn interaction is expected to be antiferromagnetic, and only the presence of a sufficient concentration of free carriers can render the antiferromagnetic Mn-Mn interaction into a ferromagnetic one.² Since Mn forms a relatively shallow acceptor level in GaAs (100 meV), the Mn impurity band merges with the valence band at sufficiently high Mn concentrations which effectively results in metallic p -type conductivity. In contrast, Mn in GaN has been experimentally observed by Korotkov *et al.*³⁶ to form a very deep state within the gap (1.4 eV). Even at very high concentrations (such as 10%) Mn will thus form merely an impurity band which will effectively pin the Fermi level and render the crystal into an insulator, as experimentally observed for our samples. (Ga,Mn)N thus resembles Mn-doped II-VI DMS in that it

fulfills the two criteria for a spin-glass, namely, randomness (since it is a diluted alloy) and frustration (which is inherent to the wurtzite lattice).

It has to be noted that, qualitatively, a superparamagnet behaves very similar to a spin-glass. Quantitatively, however, superparamagnetic materials neither exhibit a cusp in ZFC curves as sharp as that observed in Fig. 5 (because of the size distribution of the ferromagnetic clusters), nor do they follow the scaling behavior shown in Fig. 8 and the AT-like field dependence of the spin-freezing temperature shown in Fig. 9.

Finally, reports in the literature about high n -type conductivity in (Ga,Mn)N layers should be considered with great caution. First, many (Ga,Mn)N layers are grown on GaN buffer layers (which may be required for growth on sapphire), which are likely to exhibit n -type conductivity and may entirely dominate the conductivity of the sample. Second, the extraordinary Hall effect present in ferromagnetic crystals greatly complicates the analysis of Hall effect measurements. Third, if clustering occurs, the crystal is electrically inhomogeneous and cannot be analyzed in a straightforward manner by the standard van der Pauw technique. Fourth, even an actual n -type conductivity of the layer may merely indicate excessive clustering, such that the matrix is essentially depleted of Mn. In fact, we have found that samples with a Mn content below 10% but grown at high temperature (810 °C) are conducting as well as ferromagnetic, indicating that cluster formation is greatly facilitated by the high growth temperature. Considering all these points, it is evident that a reliable interpretation of the electrical properties of (Ga,Mn)N may be extremely demanding, and cannot be done without a detailed analysis of the structural and magnetic properties of the system.

V. CONCLUSIONS

We have shown that homogeneous (Ga,Mn)N is intrinsically a Heisenberg spin-glass. This discovery may have important implications for the understanding of spin-glasses in general, since it adds a new material class (an insulating wurtzite III-V compound) to the list of known spin-glasses. Where possible, we have generated quantitative results to facilitate comparison with existing theories. In fact, the comparisons made in the present paper are generally in good agreement with theory, although details may need further theoretical refinement. The ferromagnetism of (Ga,Mn)N reported in several publications is likely not to be an intrinsic property of insulating (Ga,Mn)N, but a consequence of precipitation, the microscopic nature of which remains to be unraveled. Finally, we suggest that codoping of GaN with Mn and Mg (Ref. 37) may well prove to be both scientifically fascinating and important from the point of view of applications, since the (moderate) concentration of free holes provided by the comparatively shallow Mg acceptors may turn the antiferromagnetic Mn-Mn interaction into a ferromagnetic one. If successful, such experiments would provide an invaluable test of the model developed by Dietl *et al.*²

ACKNOWLEDGMENTS

We thank J. Keller and B. Beschoten of 2. Physikalisches Institut, RWTH Aachen for high-temperature magnetization measurements and valuable discussions. We are indebted to

J. Herfort and M. Moreno for help with the SQUID setup and valuable discussions. We are grateful to C. Hucho for a critical reading of the manuscript. Part of this work has been sponsored by the Bundesministerium für Bildung und Forschung of Germany.

*Electronic address: dhar@pdi-berlin.de

- ¹S. A. Wolf, D. D. Awschalom, R. A. Buhrman, J. M. Daughton, S. von Molnár, M. L. Roukes, A. Y. Chtchelkanova, and D. M. Treger, *Science* **294**, 1488 (2001), and references therein.
- ²T. Dietl, H. Ohno, F. Matsukura, J. Cibert, and D. Ferrand, *Science* **287**, 1019 (2000).
- ³M. Zając, J. Gosk, M. Kamińska, A. Twardowski, T. Szyszko, and S. Podsiadło, *Appl. Phys. Lett.* **79**, 2432 (2001).
- ⁴S. Kuwabara, T. Kondo, T. Chikyow, P. Ahmet, and H. Munekata, *Jpn. J. Appl. Phys.* **40**, L724 (2001).
- ⁵T. Sasaki, S. Sonoda, Y. Yamamoto, K. Suga, S. Shimizu, K. Kindo, and H. Hori, *J. Appl. Phys.* **91**, 7911 (2002).
- ⁶M. L. Reed, N. A. El-Masry, H. H. Stadelmaier, M. K. Rittums, M. J. Reed, C. A. Parker, J. C. Roberts, and S. M. Bedair, *Appl. Phys. Lett.* **79**, 3473 (2001).
- ⁷G. T. Thaler, M. E. Overberg, B. Gila, R. Frazier, C. R. Abernathy, S. J. Pearton, J. S. Lee, S. Y. Lee, Y. D. Park, Z. G. Khim, J. Kim, and F. Ren, *Appl. Phys. Lett.* **80**, 3964 (2002).
- ⁸M. E. Overberg, C. R. Abernath, S. J. Pearton, N. A. Theodoropoudou, K. T. McCarthy, and A. F. Hebard, *Appl. Phys. Lett.* **79**, 1312 (2001).
- ⁹K. Sato and H. Katayama-Yoshida, *Jpn. J. Appl. Phys., Part 2* **40**, L485 (2001).
- ¹⁰M. Tanaka, J. P. Harbison, J. DeBoeck, T. Philips, T. L. Cheeks, and V. G. Keramidis, *Appl. Phys. Lett.* **62**, 1565 (1993).
- ¹¹H. Yang, H. Al-Britthen, E. Trifan, D. C. Ingan, and A. R. Smith, *J. Appl. Phys.* **91**, 1053 (2002).
- ¹²Y. Cui and L. Li, *Appl. Phys. Lett.* **80**, 4139 (2002).
- ¹³S. Dhar, O. Brandt, A. Trampert, K. Friedland, and K. H. Ploog (unpublished).
- ¹⁴S. Dhar, O. Brandt, A. Trampert, K. Friedland, K. H. Ploog, J. Keller, and B. Beschoten, *Appl. Phys. Lett.* **82**, 2077 (2003).
- ¹⁵J. K. Furdyna, *J. Appl. Phys.* **64**, R29 (1988).
- ¹⁶O. Brandt, R. Muralidharan, P. Waltereit, A. Thamm, A. Trampert, H. von Kiedrowski, and K. H. Ploog, *Appl. Phys. Lett.* **75**, 4019 (1999).
- ¹⁷A. Thamm, O. Brandt, Y. Takemura, A. Trampert, M. Ramsteiner, and K. H. Ploog, *Appl. Phys. Lett.* **75**, 944 (1999).
- ¹⁸J. Sadowski, R. Mathieu, P. Svedlindh, J. Z. Domagała, J. Bak-Misiuk, K. Świątek, M. Karlsteen, J. Kanski, L. Ilver, H. Åsklund, and U. Södervall, *Appl. Phys. Lett.* **78**, 3271 (2001); M. Moreno, A. Trampert, B. Jenichen, L. Däweritz, and K. H. Ploog, *J. Appl. Phys.* **92** (2002).
- ¹⁹H. Kett, W. Gebhardt, U. Krey, and J. K. Furdyna, *J. Magn. Magn. Mater.* **25**, 215 (1981).
- ²⁰C. Pappa, J. Hammann, and C. Jacoboni, *J. Phys. C* **17**, 1303 (1984).
- ²¹G. C. DeFotis, G. S. Coker, J. W. Jones, C. S. Branch, H. A. King, J. S. Bergman, S. Lee, and J. R. Goodey, *Phys. Rev. B* **58**, 12 178 (1998).
- ²²M. Zając, R. Doradzinski, J. Gosk, J. Szczytko, M. Lefeld-Sosnowska, M. Kamińska, M. Palczewska, E. Grzanka and W. Gębicki, *Appl. Phys. Lett.* **78**, 1276 (2001).
- ²³J. Spałek, A. Lewicki, Z. Tarnawski, J. K. Furdyna, R. R. Galazka, and Z. Obuszko, *Phys. Rev. B* **33**, 3407 (1986).
- ²⁴J. L. Tholence and R. Tournier, *J. Phys. (Paris)* **35**, C4229 (1974).
- ²⁵R. W. Knitter, J. S. Konvel, and H. Claus, *J. Magn. Magn. Mater.* **5**, 356 (1977).
- ²⁶H. Maletta and W. Felsch, *Phys. Rev. B* **20**, 1245 (1979).
- ²⁷W. Kinzel, *Phys. Rev. B* **19**, 4595 (1979).
- ²⁸A. Aharoni and E. P. Wohlfarth, *J. Appl. Phys.* **55**, 1664 (1984).
- ²⁹A. Mauger, J. Ferre, A. Ayadi, and P. Nordblad, *Phys. Rev. B* **37**, 9022 (1988).
- ³⁰A. T. Ogielski, *Phys. Rev. B* **32**, 7384 (1985).
- ³¹J. Souletie and J. L. Tholence, *Phys. Rev. B* **32**, 516 (1985).
- ³²M. Saint-Paul, J. L. Tholence, and W. Giriat, *Solid State Commun.* **60**, 621 (1986).
- ³³N. Bontemps, J. Rajchenbach, R. V. Chamberlin, and R. Orbach, *Phys. Rev. B* **30**, 6514 (1984).
- ³⁴J. R. L. De Almeida and D. J. Thouless, *J. Phys. A* **11**, 983 (1978); M. Gabay and G. Toulouse, *Phys. Rev. Lett.* **47**, 201 (1981).
- ³⁵K. H. Fischer, *Z. Phys. B: Condens. Matter* **60**, 151 (1985).
- ³⁶R. Y. Korotkov, J. M. Gregie, and B. W. Wessels, *Appl. Phys. Lett.* **80**, 1731 (2002).
- ³⁷R. Y. Korotkov, J. M. Gregie, B. Han, and B. W. Wessels, *Physica B* **308–310**, 18 (2001).